Choi et al. Nanoscale Research Letters (2017) 12:492
DOI 10.1186/s11671-017-2266-7

Nanoscale Research Letters

NANO EXPRESS Open Access

Temperature dependence of band gap in $MoSe_2$ grown by molecular beam epitaxy

Byoung Ki Choi[1], Minu Kim[2,3], Kwang-Hwan Jung[4], Jwasoon Kim[4], Kyu-Sang Yu[4] and Young Jun Chang[1*]

Abstract

We report on a temperature-dependent band gap property of epitaxial $MoSe_2$ ultrathin films. We prepare uniform $MoSe_2$ films epitaxially grown on graphenized SiC substrates with controlled thicknesses by molecular beam epitaxy. Spectroscopic ellipsometry measurements upon heating sample in ultra-high vacuum showed temperature-dependent optical spectra between room temperature to 850 °C. We observed a gradual energy shift of optical band gap depending on the measurement temperature for different film thicknesses. Fitting with the vibronic model of Huang and Rhys indicates that the constant thermal expansion accounts for the steady decrease of band gap. We also directly probe both optical and stoichiometric changes across the decomposition temperature, which should be useful for developing high-temperature electronic devices and fabrication process with the similar metal chalcogenide films.

Keywords: $MoSe_2$, Temperature-dependent band gap, Thermal stability, Molecular beam epitaxy, Spectroscopic ellipsometry, Time of flight medium-energy ion-scattering spectroscopy

Background

Two-dimensional layered transition metal dichalcogenides (TMDs) have attracted amplified interests due to interesting physical behaviors such as direct-indirect band gap transition, valleytronics, ferroelectric, and charge-density wave [1–7]. Many semiconducting TMDs possess direct band gap at the K point in monolayer (ML), so that the strong excitonic transition [8–17], and the resulting enhancement of optical behavior for optoelectronic device development are exhibited [18–25]. Especially, the direct band gap (1.55 eV) of $MoSe_2$ is close to the optimal band gap value of single-junction solar cells and photo-electrochemical devices [26–30]. In addition, variation of band gap via partial oxidation or temperature control provides potential applications involving external control of optical properties in TMDs, such as optoelectronic devices toward wider light spectrum [31, 32]. However, modulation of band gap has been studied so far by monitoring A exciton peaks in 1-ML $MoSe_2$ below 420 K [26], and high-temperature stability has not been addressed for any TMD films. This is partly due to difficulty in preparation of single crystalline TMD films with large uniformity.

Growth of TMD film has been rapidly developing to meet the elevated interests for various ways, such as chemical vapor deposition (CVD), pulsed laser deposition, and molecular beam epitaxy (MBE) [5, 33–35]. CVD has been most widely utilized for crystalline films, but it often provides non-uniform films with small crystalline grains. The state-of-the-art metal-organic CVD growth shows uniform films with polycrystalline grains [36]. On the other hand, MBE has been proved to grow epitaxial films with uniformity for various kinds of TMDs. In addition, in situ reflection high-energy electron diffraction (RHEED) monitoring provides precise control of film thicknesses.

In this paper, we report on the high-temperature optical and stoichiometry properties of epitaxial $MoSe_2$ ultrathin films grown by MBE. We analyzed temperature dependence of the band gap of the $MoSe_2$ ultrathin films with spectroscopic ellipsometry. We also directly measure the decomposition process in terms of surface crystallinity and stoichiometry.

Methods

Series of $MoSe_2$ films were epitaxially grown on graphenized SiC substrates in a home-built MBE system with

* Correspondence: yjchang@uos.ac.kr
[1]Department of Physics, University of Seoul, Seoul 02504, Republic of Korea
Full list of author information is available at the end of the article

base pressures of 1×10^{-10} Torr. We used 6H-SiC single crystal substrates, supplied by the Crystal Bank at Pusan National University. We prepared bilayer graphene on the 6H-SiC substrates by annealing at 1300 °C for ~5 min, following the reported recipe [1]. On the graphene surface, we grew epitaxial $MoSe_2$ films with lattice mismatch of ~0.3%. Molybdenum and selenium were evaporated with e-beam evaporator and effusion cell, respectively. We deposited the films at growth temperature of 250 °C with growth rate of 0.1 ML/min, followed with post-annealing at 600 °C for 30 min [1]. We monitor the film surface with in situ reflection high-energy electron diffraction (RHEED) with high voltage of 18 kV.

Film crystallinity was checked with high-resolution x-ray diffraction (HRXRD, Bruker, D8 Discover). Spectroscopic reflection measurement was performed with two spectroscopic ellipsometries (JA Woollam, V-VASE), one in atmosphere and the other in a separate ultra-high vacuum chamber. Stoichiometry was analyzed by time of flight medium-energy ion-scattering spectroscopy (TOF-MEIS, KMAC, MEIS-K120) with He^+ ion beam with 100.8 keV. For estimation of sample thickness, we used bulk density values for SiC with 3.21 g/cm^3 and for $MoSe_2$ with 6.98 g/cm^3.

Results and discussion

We fabricated three kinds of epitaxial $MoSe_2$ films with different thicknesses (1, 2.5, and 16 ML) on graphene/SiC substrates. In Fig. 1, RHEED images shows epitaxially grown $MoSe_2$ films. Well-separated straight lines in Fig. 1a, b indicate electron diffraction from the well-ordered surface crystallinity. Additional lines with different periodicity correspond to the diffraction signal from the underlying graphene probably due to electron penetration through the ultrathin films, which is consistent with the previous reports on MBE-grown $MoSe_2$ films [1]. As the film thickness increases, we found a weaker RHEED signal along with rounded spots, which implies in-plane orientation disorder at the surface of the 16-ML film, as shown in Fig. 1c. Figure 1d shows HRXRD pattern of the 16-ML film, which shows only *c*-axis ordered peaks, i.e., (00n), except the very sharp peaks originated from the single crystalline SiC wafer. These *c*-axis diffraction peaks indicate that the 16-ML film possesses periodic layer stacking, even though the top surface may have in-plane disorders. Therefore, we prepared all three epitaxial films with high crystallinity, which are ready for temperature-dependent analysis.

We first obtained room temperature optical spectra of the 16 ML-thick $MoSe_2$ both in air and in UHV condition with two distinct ellipsometry spectrometers. As shown in Fig. 2c, f, those two spectra (solid and dashed lines) well overlap and show two characteristic peaks near ~1.5 eV (A) and ~1.7 eV (B). Those two peaks correspond to the two excitonic transitions at the K point of the band structure [37, 38]. Strong spin-orbit coupling induces splitting of degenerated valence band maximum at K point [29, 39–42]. These two exciton peak energies well compared to the reported exciton energy values, ~1.55 and ~1.75 eV, in the exfoliated bulk [38]. Then, we show ellipsometry spectra of the 1- and 2.5-ML samples

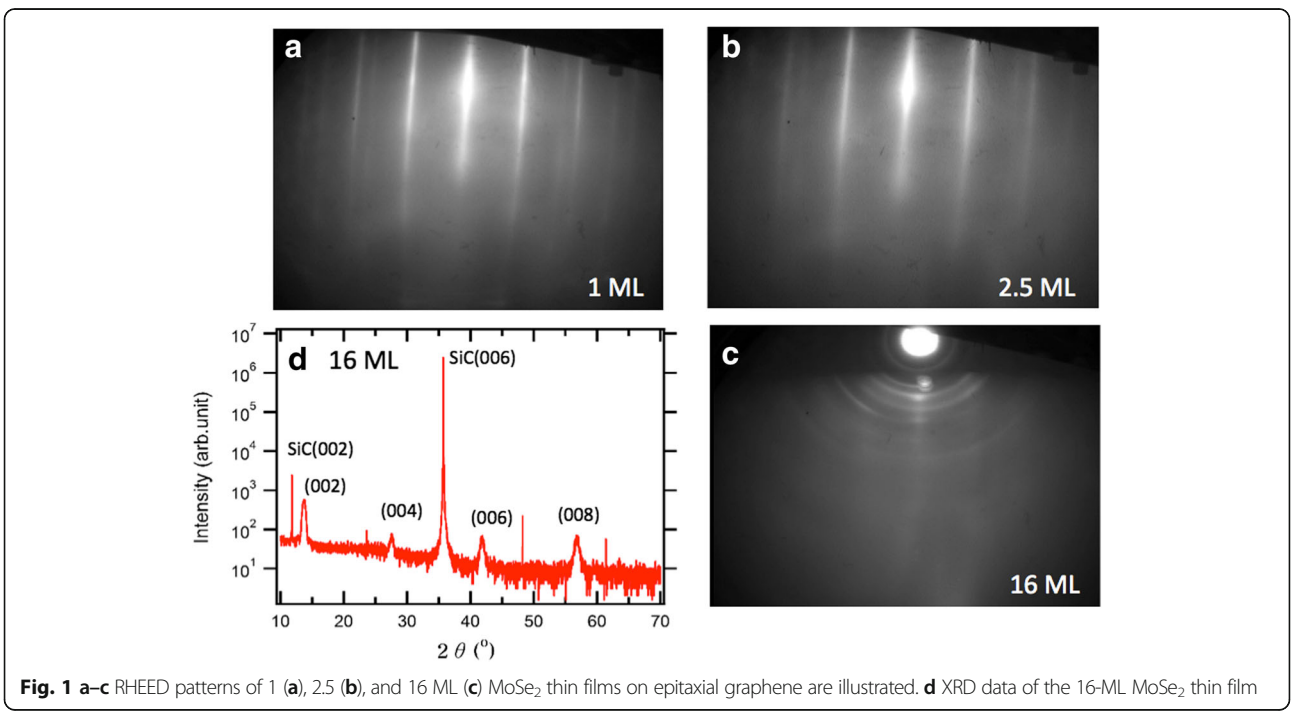

Fig. 1 a–c RHEED patterns of 1 (**a**), 2.5 (**b**), and 16 ML (**c**) $MoSe_2$ thin films on epitaxial graphene are illustrated. **d** XRD data of the 16-ML $MoSe_2$ thin film

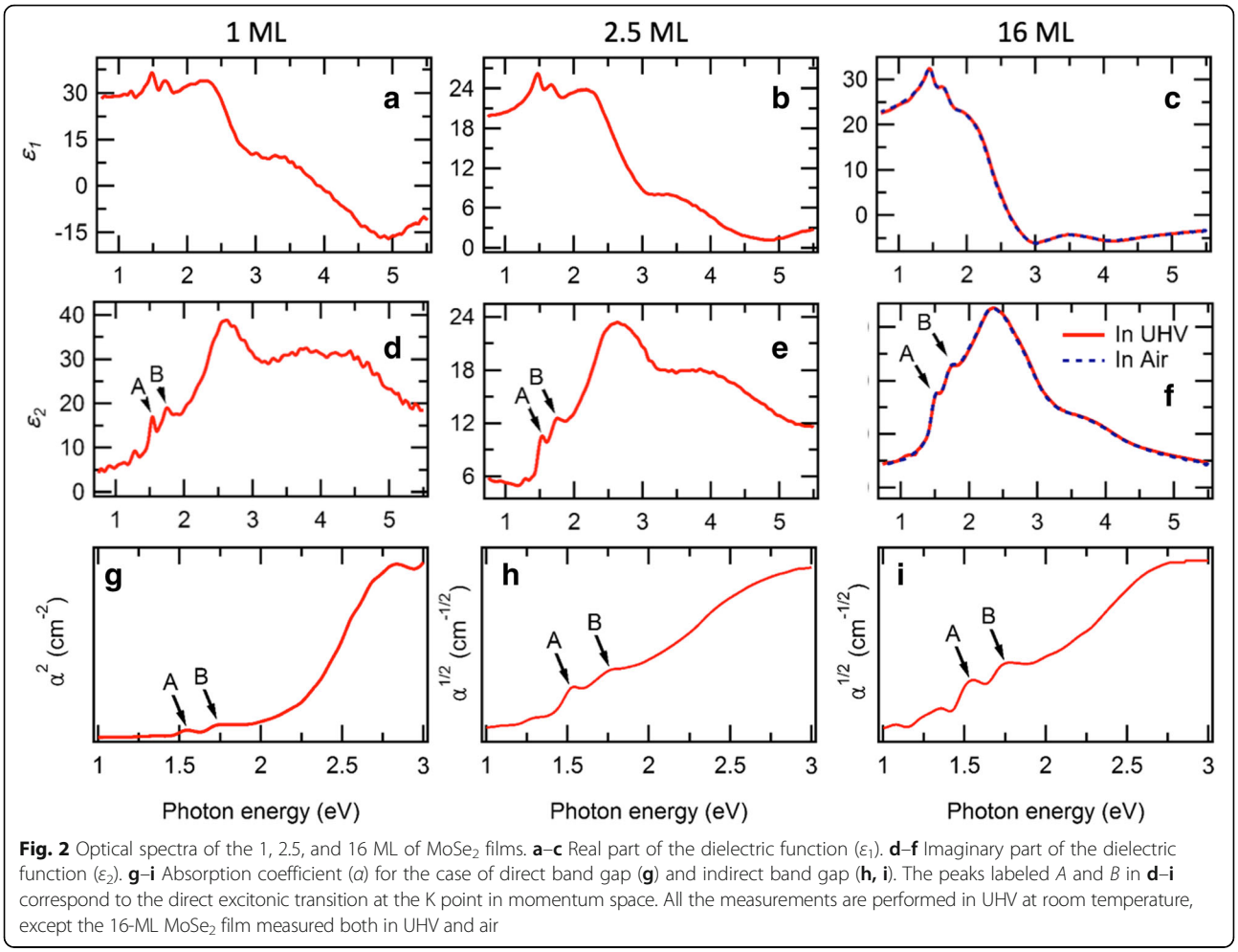

Fig. 2 Optical spectra of the 1, 2.5, and 16 ML of $MoSe_2$ films. **a**–**c** Real part of the dielectric function (ε_1). **d**–**f** Imaginary part of the dielectric function (ε_2). **g**–**i** Absorption coefficient (α) for the case of direct band gap (**g**) and indirect band gap (**h, i**). The peaks labeled *A* and *B* in **d**–**i** correspond to the direct excitonic transition at the K point in momentum space. All the measurements are performed in UHV at room temperature, except the 16-ML $MoSe_2$ film measured both in UHV and air

measured in UHV condition at room temperature, as shown in Fig. 2a–e, respectively. As the film thickness is reduced, the exciton peaks become sharp, probably due to band structure transition from the indirect band gap to the direct one [1, 43]. The ellipsometry spectrum of the 1 ML resembles the reported spectrum of exfoliated 1-ML $MoSe_2$ flake [38, 44]. However, the ellipsometry spectrums of few layers-thick $MoSe_2$ have yet to be reported. From the ellipsometry spectra, we extracted the two exciton peak energies of all three samples at room temperature. As listed in Table 1, both the A and B exciton peaks show negligible change as the layer thickness decreases, because it relates with the direct band gap, which is insensitive to the thickness-dependent direct-indirect band gap transition. The A exciton band gap (1.54 eV) of the 1-ML sample is close to the values reported in the photoluminescence experiments on mechanically exfoliated [26] and CVD-grown 1-ML $MoSe_2$ on SiO_2 [31, 45], and the ARPES experiments of MBE-grown 1-ML $MoSe_2$ on graphene [1].

To extract optical band gap values using Tauc plot, we further converted the ellipsometry spectra into the absorption coefficient α of each samples. Since only the 1-ML $MoSe_2$ has a direct band gap, we manifest α^2 and $\alpha^{1/2}$ to estimate the band gap for the 1 ML and the rest of the samples, respectively. As shown in Fig. 2g–i, the absorption spectra also show the two exciton peaks between 1.5–1.75 eV, which is consistent with the reported

Table 1 Exciton peak energies and the fitting parameters from Eq. (1) for the 1, 2.5, and 16 ML of $MoSe_2$ films

Layer thickness (ML)	A exciton (eV, 300 K)	B exciton (eV, 300 K)	E_g(300 K) (eV)	Electron-phonon coupling (S)	E_g(0) (eV)	Average phonon energy (meV)
1	1.54	1.75	2.18	3.5	2.32	11.6
2.5	1.53	1.76	1.54	3	1.68	
16	1.54	1.76	1.40	4	1.50	

absorption spectrum of 1-ML $MoSe_2$ grown by CVD [44]. In addition to the two exciton peaks, the absorption spectra show a broad peak centered at ~3 eV, corresponding to the charge transfer absorption, and we could extract band gap value using Tauc plot, which is used to determine optical band gap in semiconductors, shown as straight line fittings in Fig. 2g–i. We listed the extracted optical band gap (E_g(300 K)) at room temperature in Table 1, in which the 1-ML value (2.18 eV) is nearly same with the reported band gap measured by scanning tunneling spectroscopy measurements [40]. Contrary to the excition peaks, the optical band gap shows sharp increase when the layer thickness is diminished. Especially, big change of band gap between 1 ML (2.18 eV) and 2.5 ML (1.54 eV) is consistent with the direct-indirect band gap transition in this ML limit [1].

To understand thermal change of the optical band gap, we repeated the ellipsometry measurements while heating the three samples in UHV condition. Figure 3 shows the series of optical spectra for various measurement temperatures ranging from room temperature to 750–850 °C. For every sample, the spectra suddenly lose the characteristic peak structures and become monotonic above different temperatures, which we define as the decomposition temperature (T_{dec}) for each sample, as we discuss stoichiometry analysis below. T_{dec} increases from 700 °C for the 1 ML to 725 °C for the 16 ML. As shown in Fig. 4a, the T_{dec} of the ultrathin films in UHV are far lower than those of bulk in air (1200 °C) [46] and in UHV (980 °C) [47]. This implies that the ultrathin $MoSe_2$ should be handled for restricted temperature range below the T_{dec}. When cooled after the thermal annealing cycles below the T_{dec}, we confirmed restoration of the optical spectra for the 2.5-ML $MoSe_2$ (see Additional file 1: Figure S1).

Below the T_{dec}, we identified gradual red shifts of the most characteristic peaks for all the three samples, as shown in Fig. 3. As shown in Fig. 4b, we extract the band gap values from the A exciton peak positions as a function of measurement temperature (also see Additional file 1: Figure S2). The temperature dependence of the A exciton peak shows nearly linear dependence, which is similar to the one in the exfoliated monolayer for 300–420 K [26]. However, the optical band gap of $MoSe_2$ is known to be quite different from the exciton peak due to exceptionally large exciton-binding energy [40].

The linear temperature dependence of the optical band gap over wide temperature range is illustrated in Fig. 4c. Repeating the Tauc plot in Fig. 2g–i, we could extract the optical band gap values from each spectra. All three samples show nearly similar linear dependence of the band gap for the wide temperature range. The linear temperature dependence of the band gap over wide temperature range is similar to one of the other semiconductors [48–51]. We could fit this temperature dependence by using the vibronic model of Huang and Rhys [51, 52];

$$E_g(T) = E_g(0) - S < h\nu > [\coth(< h\nu > /2k_BT) - 1] \quad (1)$$

where $E_g(0)$ is the band gap at 0 K, S is a dimensionless electron-phonon coupling parameter, $<h\nu>$ is the average acoustic phonon energy, and the coth term represents the density of phonons at the specific temperature. Shown as dashed lines in Fig. 4c, we could fit the temperature dependence well with $E_g(0)$ = 1.5–2.32 eV and S = 3–4, while we fixed the value of $<h\nu>$ = 11.6 meV from the previously reported value in the exfoliated monolayer $MoSe_2$ [26]. While the fitting parameters are listed in Table 1, the parameters are quite different from the reported values ($E_g(0)$ = 1.64 eV and S = 1.93) for the exfoliated monolayer $MoSe_2$, because they fit the A exciton energy instead of the optical band gap. However, S values are quite similar to the reported values for three-dimensional compound semiconductors, such as GaAs

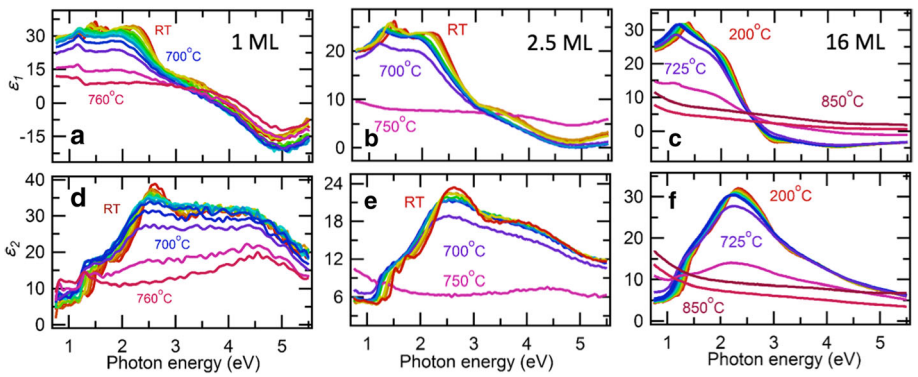

Fig. 3 Temperature dependence of optical spectra of the 1, 2.5, and 16 ML of $MoSe_2$ films. **a**–**c** Real part of the dielectric function (ε_1). **d**–**f** Imaginary part of the dielectric function (ε_2)

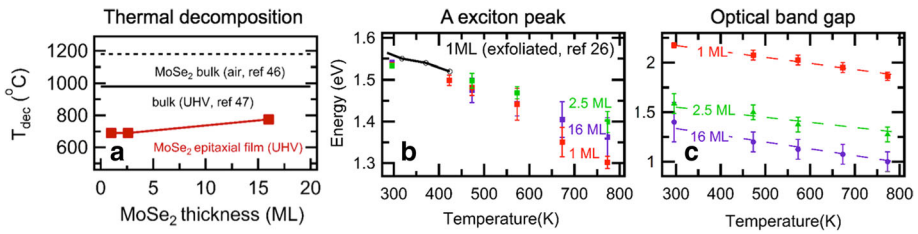

Fig. 4 **a** T_{dec} of $MoSe_2$ bulk and thin films in air or UHV conditions. *Red squares* are from the temperature-dependent optical spectra on the $MoSe_2$ epitaxial films, while *black solid* and *dashed lines* correspond to the bulk $MoSe_2$ in UHV [47] and air [46] condition in the literatures. **b** Temperature dependence of the A exciton peaks in imaginary part of dielectric functions in Fig. 3d–f. *Black open circles* indicate the A exciton peak values of the exfoliated 1-ML $MoSe_2$ taken in the previous report [26]. **c** Temperature dependence of the optical band gap values for the 1, 2.5, and 16 ML of $MoSe_2$ films, taken from the absorption spectra

and GaP [48]. We note that nearly constant thermal expansion coefficient of $MoSe_2$ above 150 K explains the linear reduction of band gap upon heating [53].

To understand the abrupt change of the optical spectra above the T_{dec} in Fig. 3, we further analyzed surface crystallinity and stoichiometry by utilizing RHEED and TOF-MEIS on the separately prepared 2-ML films, as shown in Fig. 5. The RHEED images show dramatic changes among the samples with different post-annealing temperatures (850, 720, 600 °C) in UHV environment. The sample annealed at 600 °C maintains the similar streaky pattern with the as-grown samples, shown as Fig. 1a, b. However, the 720 °C sample shows additional spots, and the 850 °C sample shows no diffraction signal due to lack of long-range crystalline order. To analyze the amount of decomposition, we performed TOF-MEIS on the 720 and 600 °C samples. The raw spectra in Fig. 5d show similar features except the ratio difference between the Se and Mo peaks between 80 and 90 keV. After modeling with assumption of uniform slab geometry and bulk densities, we obtained depth profile of chemical stoichiometry for both samples. As shown in Fig. 5f, the 600 °C sample shows 1:2 ratio for Mo and Se and the film thickness of ~1.3 nm, indicating preserving the stoichiometry of the as-grown state up to 600 °C. However, the 720 °C sample shows reduced ratio of 1:1.7 and increased thickness of ~1.6 nm, indicating selenium deficiency and surface roughening upon heating across the T_{dec}. Therefore, the $MoSe_2$ layer begins to disorder and decompose at 720 °C, and then remains a disordered molybdenum layer in 850 °C. These direct evidences should be helpful for designing high-temperature fabrication process based on the similar kinds of metal chalcogenide films.

Conclusions

We prepared a set of $MoSe_2$ ultrathin films epitaxially grown by MBE. From the temperature-dependent optical spectra between room temperature to ~850 °C, we identified the thickness-dependent T_{dec} and the temperature dependence of band gap. The linear decrease of the band gap is well understood with the vibronic model of Huang and Rhys. Such high-temperature characters should play an important role for development of electronic and optoelectronic devices based on the related metal chalcogenide films.

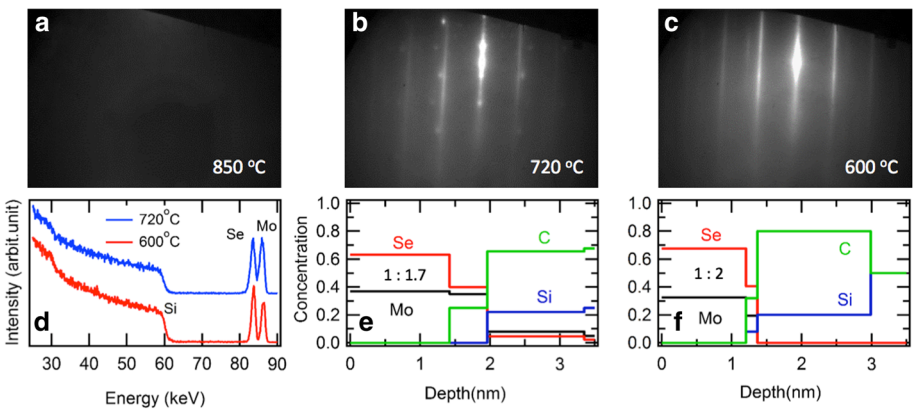

Fig. 5 **a–c** RHEED pattern of the 2-ML $MoSe_2$ films after annealing at 850 (**a**), 720 (**b**), and 600 °C (**c**) in UHV condition. **d** TOF-MEIS spectra of the 2-ML $MoSe_2$ films after annealing at 720 °C (*blue*) and 600 °C (red). **e, f** Depth profile of chemical composition of the annealed films at 720 °C (**e**) and 600 °C (**f**), obtained from the TOF-MEIS analysis. Note that the stoichiometric ratio of Mo:Se is 1:1.7 and 1:2 for the 720 and 600 °C samples, respectively

Additional file

Additional file 1: Figure S1 a, b. Optical spectra (ε_2 (a) and ε_2 (b)) of 2.5-ML $MoSe_2$ at 100 °C cooled after thermal annealing at the indicated temperatures. The spectra remain nearly same up to 650, indicating that the observed spectral changes in Fig. 3 are mostly due to the reproducible thermal effect. Figure S2 Expanded plot of temperature dependent optical spectra of the 1, 2.5, and 16 ML of $MoSe_2$ films to show detailed thermal shifts; a-c Real part of the dielectric function (ε_1), d-f Imaginary part of the dielectric function (ε_2). (DOCX 482 kb)

Abbreviations

CVD: Chemical vapor deposition;; $E_g(0)$: Band gap at 0 K;; $E_g(300\ K)$: Band gap at 300 K;; HRXRD: High-resolution x-ray diffraction;; MBE: Molecular beam epitaxy;; RHEED: Reflection high-energy electron diffraction;; T_{dec}: Decomposition temperature;; TMD: Transition metal dichalcogenide;; TOF-MEIS: Time of flight medium-energy ion-scattering spectroscopy;

Acknowledgements

Authors thank Gideok Kim and Tae Dong Kang for ellipsometry measurements. This work is supported by the National Research Foundation of Korea (NRF) grants funded by the Korean government (MSIP) (NRF-2017R1C1B2004927). This work was supported by the Research Center Program of the Institute for Basic Science in Korea (Grant No. IBS-R009-D1).

Authors' contributions

YJC designed the experiments. BKC performed the sample preparations. BKC, MK, KHJ, JK, and KSY performed the sample characterizations. BKC and YJC analyzed the results and wrote the manuscript. All authors read and approved the final manuscript.

Ethics approval and consent to participate

Not applicable

Consent for publication

Not applicable

Competing interests

The authors declare that they have no competing interests.

Publisher's Note

Author details

[1]Department of Physics, University of Seoul, Seoul 02504, Republic of Korea. [2]Center for Correlated Electron Systems, Institute for Basic Science (IBS), Seoul 08826, Republic of Korea. [3]Department of Physics and Astronomy, Seoul National University, Seoul 08826, Republic of Korea. [4]Korea Materials and Analysis Corp, Daejeon 34028, Republic of Korea.

Received: 22 May 2017 Accepted: 3 August 2017
Published online: 15 August 2017

References

1. Zhang Y et al (2014) Direct observation of the transition from indirect to direct bandgap in atomically thin epitaxial MoSe2. Nat Nanotechnol 9(2): 111–115
2. Elias AL et al (2013) Controlled synthesis and transfer of large-area WS2 sheets: from single layer to few layers. ACS Nano 7(6):5235–5242
3. Zhang Y et al (2013) Controlled growth of high-quality monolayer WS2 layers on sapphire and imaging its grain boundary. ACS Nano 7(10): 8963–8971
4. Lee YH et al (2012) Synthesis of large-area MoS2 atomic layers with chemical vapor deposition. Adv Mater 24(17):2320–2325
5. Mo S-K (2017) Angle-resolved photoemission spectroscopy for the study of two-dimensional materials. Nano Convergence 4(1):6
6. Chen P, Chan YH, Fang XY, Zhang Y, Chou MY, Mo SK, Chiang TC (2015) Charge density wave transition in single-layer titanium diselenide. Nature Commun 6:8943.
7. Strocov VN, Shi M, Kobayashi M, Monney C, Wang X, Krempask J, Blaha P (2012) Three-dimensional electron realm in VSe 2 by Soft-X-Ray photoelectron Spectroscopy: Origin of charge-density waves. Phys Rev Lett 109(8):086401
8. Chernikov A et al (2014) Exciton binding energy and nonhydrogenic Rydberg series in monolayer WS 2. Phys Rev Lett 113(7):076802
9. He K et al (2014) Tightly bound excitons in monolayer WSe 2. Phys Rev Lett 113(2):026803
10. Mak KF et al (2013) Tightly bound trions in monolayer MoS2. Nat Mater 12(3):207–211
11. Ramasubramaniam A (2012) Large excitonic effects in monolayers of molybdenum and tungsten dichalcogenides. Phys Rev B 86(11):115409
12. Zhu B, Chen X, Cui X (2015) Exciton binding energy of monolayer WS2. Sci Rep 5:9218
13. Zhu C et al (2014) Exciton valley dynamics probed by Kerr rotation in WSe 2 monolayers. Phys Rev B 90(16):161302
14. Li Z et al (2015) Active light control of the MoS2 monolayer exciton binding energy. ACS Nano 9(10):10158–10164
15. Ross JS et al (2013) Electrical control of neutral and charged excitons in a monolayer semiconductor. Nat Commun 4:1474
16. Dufferwiel S, et al (2015) Exciton–polaritons in van der Waals heterostructures embedded in tunable microcavities. Nature Commun 6:8579
17. Qiu DY, Felipe H, Louie SG (2013) Optical spectrum of MoS 2: many-body effects and diversity of exciton states. Phys Rev Lett 111(21):216805
18. Jo S et al (2014) Mono-and bilayer WS2 light-emitting transistors. Nano Lett 14(4):2019–2025
19. Sundaram R et al (2013) Electroluminescence in single layer MoS2. Nano Lett 13(4):1416–1421
20. Yin Z et al (2011) Single-layer MoS2 phototransistors. ACS Nano 6(1):74–80
21. Pankove JI (1971) Optical processes in semiconductors. Prentice-Hall, Englewood Cliffs: Courier Corporation
22. Xia F et al (2014) Two-dimensional material nanophotonics. Nat Photonics 8(12):899–907
23. Shen W-C, Chen R-S, Huang Y-S (2016) Photoconductivities in MoS2 nanoflake photoconductors. Nanoscale Res Lett 11(1):124
24. Hsiao Y-J et al (2015) Red-shift effect and sensitive responsivity of MoS2/ZnO flexible photodetectors. Nanoscale Res Lett 10(1):443
25. Ye J et al (2015) A facile way to fabricate high-performance solution-processed n-MoS2/p-MoS2 bilayer photodetectors. Nanoscale Res Lett 10(1):454
26. Tongay S et al (2012) Thermally driven crossover from indirect toward direct bandgap in 2D semiconductors: MoSe2 versus MoS2. Nano Lett 12(11): 5576–5580
27. Shi Y et al (2013) Highly ordered mesoporous crystalline MoSe2 material with efficient visible-light-driven photocatalytic activity and enhanced lithium storage performance. Adv Funct Mater 23(14):1832–1838
28. Tributsch H (1978) The MoSe2 electrochemical solar cell: anodic coupling of electron transfer to d→ d photo-transitions in layer crystals. Ber Bunsenges Phys Chem 82(2):169–174
29. Coehoorn R, Haas C, De Groot R (1987) Electronic structure of MoSe 2, MoS 2, and WSe 2. II. The nature of the optical band gaps. Phys Rev B 35(12):6203
30. Coehoorn R et al (1987) Electronic structure of MoSe 2, MoS 2, and WSe 2. I. Band-structure calculations and photoelectron spectroscopy. Phys Rev B 35(12):6195
31. Song SH et al (2015) Bandgap widening of phase quilted, 2D MoS2 by oxidative intercalation. Adv Mater 27(20):3152–3158
32. Cardona M, Yu PY (1996) Fundamentals of semiconductors. Springer-Verlag.
33. Han SA, Bhatia R, Kim S-W (2015) Synthesis, properties and potential applications of two-dimensional transition metal dichalcogenides. Nano Convergence 2(1):17
34. Wang F et al (2015) Synthesis, properties and applications of 2D non-graphene materials. Nanotechnology 26(29):292001
35. Choi BK et al (2017) Tunable wetting property in growth mode-controlled WS 2 thin films. Nanoscale Res Lett 12(1):262
36. Kang K et al (2015) High-mobility three-atom-thick semiconducting films with wafer-scale homogeneity. Nature 520(7549):656–660
37. Wilson J, Yoffe A (1969) The transition metal dichalcogenides discussion and interpretation of the observed optical, electrical and structural properties. Adv Phys 18(73):193–335

38. Li Y et al (2014) Measurement of the optical dielectric function of monolayer transition-metal dichalcogenides: MoS2, MoSe2, WS2, and WSe2. Phys Rev B 90(20):205422
39. Alidoust N et al (2014) Observation of monolayer valence band spin-orbit effect and induced quantum well states in MoX2. Nat Commun 5
40. Ugeda MM et al (2014) Giant bandgap renormalization and excitonic effects in a monolayer transition metal dichalcogenide semiconductor. Nat Mater 13(12):1091–1095
41. Zhu Z, Cheng Y, Schwingenschlögl U (2011) Giant spin-orbit-induced spin splitting in two-dimensional transition-metal dichalcogenide semiconductors. Phys Rev B 84(15):153402
42. Molina-Sánchez A et al (2013) Effect of spin-orbit interaction on the optical spectra of single-layer, double-layer, and bulk MoS2. Phys Rev B 88(4):045412
43. Ellis JK, Lucero MJ, Scuseria GE (2011) The indirect to direct band gap transition in multilayered MoS2 as predicted by screened hybrid density functional theory. Appl Phys Lett 99(26):261908
44. Liu H-L et al (2014) Optical properties of monolayer transition metal dichalcogenides probed by spectroscopic ellipsometry. Appl Phys Lett 105(20):201905
45. Lu X et al (2014) Large-area synthesis of monolayer and few-layer MoSe2 films on SiO2 substrates. Nano Lett 14(5):2419–2425
46. Brainard, W.A., The thermal stability and friction of the disulfides, diselenides, and ditellurides of molybdenum and tungsten in vacuum. 1969
47. Hayne W (2011) Melting, boiling, triple, and critical points of the elements. In: CRC handbook of chemistry and physics, 92nd edn. CRC Press, Boca Raton(2011–2012, pp 4–122
48. Panish M, Casey H Jr (1969) Temperature dependence of the energy gap in GaAs and GaP. J Appl Phys 40(1):163–167
49. Bludau W, Onton A, Heinke W (1974) Temperature dependence of the band gap of silicon. J Appl Phys 45(4):1846–1848
50. Clark CD, Dean PJ, Harris PV (1964) Intrinsic edge absorption in diamond. Proc R Sot A 277: Mathematical, Physical and Engineering Sciences, p 312
51. O'Donnell K, Chen X (1991) Temperature dependence of semiconductor band gaps. Appl Phys Lett 58(25):2924–2926
52. Huang K, Rhys A (1950) Theory of light absorption and non-radiative transitions in F-centres. Proc R Soc. London, Ser. A 204: Mathematical, Physical and Engineering Sciences. The Royal Society, p 406
53. Sevik C (2014) Assessment on lattice thermal properties of two-dimensional honeycomb structures: graphene, h-BN, h-MoS2, and h-MoSe2. Phys Rev B 89(3):035422